

Article

Diffusional Behavior of New Insulating Gas Mixtures as Alternatives to the SF₆-Use in Medium Voltage Switchgear

Ane Espinazo ^{1,*}, José Ignacio Lombrana ¹, Estibaliz Asua ², Beñat Pereda-Ayo ¹, María Luz Alonso ³, Rosa María Alonso ³, Leire Cayero ¹, Jesús Izcara ⁴ and Josu Izagirre ⁴

¹ Chemical Engineering Department, Faculty of Science and Technology, University of the Basque Country (UPV/EHU), Barrio Sarriena s/n, 48940 Leioa, Spain; ji.lombrana@ehu.eu (J.I.L.); benat.pereda@ehu.eu (B.P.-A.); leirecayerogaray@gmail.com (L.C.)

² Electricity and Electronics Department, Faculty of Science and Technology, University of the Basque Country (UPV/EHU), Barrio Sarriena s/n, 48940 Leioa, Spain; estibaliz.asua@ehu.eu

³ Analytical Chemistry Department, Faculty of Science and Technology, University of the Basque Country (UPV/EHU), Barrio Sarriena s/n, 48940 Leioa, Spain; marialuz.alonso@ehu.eu (M.L.A.); rosamaria.alonso@ehu.eu (R.M.A.)

⁴ Ormazabal Corporate Technology, Parque Empresarial Boroa, Parcela 24, 48340 Amorebieta-Etxano, Spain; jih@ormazabal.com (J.I.); josu.izagirre@ormazabal.com (J.I.)

* Correspondence: ane.espinazo@ehu.eu

Abstract: Regarding the use of SF₆ in medium voltage switchgear (MVS), a review of alternatives was encouraged by the European Parliament in Regulation No 517/2014. This is aimed at a new regulatory change, that is expected soon, which will include its prohibition, similar to what has happened with other fluorinated greenhouse gases in other fields, like refrigeration. Therefore, there is an urgent need to study the physical and chemical properties of alternative gas mixtures to determine if they are suitable to replace SF₆. In this context, this work addresses the diffusional analysis of new gases. Binary and ternary mixtures made of 1,3,3,3-tetrafluoropropene (C₃F₄H₂) and heptafluoroisopropyl trifluoromethyl ketone (C₅F₁₀O), using dry air as a carrier gas, were studied. The mixtures were analyzed using original equipment, composed of UV-Vis spectroscopy technology in a sealed gas chamber, which is similar to MVS. Consequently, an experimental equipment that monitors the concentration of a gas mixture online and a model that predicts the mixing process were designed and tested. The concentration profiles were obtained concerning both the time and position in the gas chamber, and the diffusional and convectional parameters were numerically calculated and optimized in an algorithm created in Scilab.

Keywords: medium voltage switchgear; SF₆ alternatives; UV-Vis spectroscopy; gas mixing modeling; multicomponent diffusion analysis



Citation: Espinazo, A.; Lombrana, J.I.; Asua, E.; Pereda-Ayo, B.; Alonso, M.L.; Alonso, R.M.; Cayero, L.; Izcara, J.; Izagirre, J. Diffusional Behavior of New Insulating Gas Mixtures as Alternatives to the SF₆-Use in Medium Voltage Switchgear. *Appl. Sci.* **2022**, *12*, 1436. <https://doi.org/10.3390/app12031436>

Academic Editor: Andreas Fischer

Received: 27 December 2021

Accepted: 27 January 2022

Published: 28 January 2022

Publisher's Note: MDPI stays neutral with regard to jurisdictional claims in published maps and institutional affiliations.



Copyright: © 2022 by the authors. Licensee MDPI, Basel, Switzerland. This article is an open access article distributed under the terms and conditions of the Creative Commons Attribution (CC BY) license (<https://creativecommons.org/licenses/by/4.0/>).

1. Introduction

Sulfur hexafluoride, SF₆, is the most widely applied gas in the electric market for insulation and electric arc quenching due to its high stability, high dielectric strength, and non-toxicity [1]. It is commonly used in gas-insulated switchgear (GIS), gas-insulated transformers (GIT), gas-insulated lines (GIL), and gas-insulated circuit breakers (GICB) [2]. However, it is also considered a very strong greenhouse gas, with a global warming potential (GWP) of about 23,500 on a 100-year horizon, making SF₆ the compound with the highest value according to the Fifth Assessment Report (AR5) of the Intergovernmental Panel on Climate Change (IPCC) [3]. In 1997, in the Kyoto Protocol [4], the reduction of greenhouse gas emissions was established, which included SF₆, so alternative gases for applications that use SF₆ have been investigated ever since. Although the equipment in which sulfur hexafluoride is used is sealed, leaks between the sealing surfaces, permeation of the gas through the thermoplastic materials, or accidents can happen [5], resulting in gas

emissions. SF₆ and other common fluorinated greenhouse gases, their lifetime (*LT*) in the atmosphere, *GWP* values, and applications are shown in Table 1.

Table 1. The lifetime (*LT*) in the atmosphere, global warming potential values in a 100-year horizon (*GWP*₁₀₀), and applications of SF₆ and other fluorinated greenhouse gases.

Component	<i>LT</i> (yr) *	<i>GWP</i> ₁₀₀ *	Application
Sulfur hexafluoride SF ₆	3200	23,500	Electrical insulation, polycrystalline silicone layer etching, blanketing gas for aluminum or magnesium [1]
Nitrogen trifluoride NF ₃	500	16,100	Microelectronic equipment cleaning, etching in microelectronics, liquid crystal displays, photovoltaic cells [6]
Difluoromethane CH ₂ F ₂	5.2	677	Refrigeration [7]
Perfluoromethane CF ₄	50,000	6630	Semiconductor manufacturing, microelectronic equipment cleaning, etching in microelectronics, chemical vapor decomposition [8]
1,1,1,2-tetrafluoroethane CF ₃ CHF ₂	28.2	3170	Refrigeration, propellant applications, vapor-phase solvent, electronic degreasing [9]
Perfluoroethane C ₂ F ₆	10,000	11,100	Semiconductor manufacturing, microelectronic equipment cleaning, etching in microelectronics, chemical vapor decomposition [8]
1,1,1,3,3-pentafluoropropane CF ₃ CH ₂ CHF ₂	7.7	858	Chemical blowing agent, refrigerant [10]
Perfluoropropane C ₃ F ₈	2600	8900	Refrigeration, semiconductor manufacturing, microelectronic equipment cleaning, etching in microelectronics, chemical vapor decomposition [8]

* Data retrieved from the Fifth Assessment Report (AR5) of the Intergovernmental Panel on Climate Change (IPCC) [3].

In 2014, the European Parliament developed Regulation (EU) No 517/2014 [11], on fluorinated greenhouse gases, where rules for the use, containment, recovery, and destruction of some fluorinated greenhouse gases are collected. These fluorinated gases include not only SF₆, but also hydrofluorocarbons (HFC) and perfluorocarbons (PFC). The European Commission is currently reviewing the impact that the actual regulation has had, and is expected to propose a new regulation soon [12]. For that reason, it is urgent to find an alternative that replaces SF₆ in medium voltage switchgear (MVS) before a possible ban on its use comes into force.

Initially, SF₆ alternatives were focused on the use of existing technologies such as air-insulated switchgear (AIS) [13] or solid-insulated switchgear (SIS) [14]. Even though both have been commonly used in low-voltage equipment, their use in higher voltage systems would require higher dimensions and, therefore, higher costs.

The mixture between SF₆ with a carrier gas, like air, N₂, or CO₂, was then considered for insulation [15]. Although the use of SF₆ is reduced, the environmental impact of the mixture, even with low SF₆ concentrations, is still significantly high. Consequently, researchers are more focused on finding other gas or gas mixtures that replace SF₆ completely.

There are some important requirements that this gas or gas mixture must meet, according to Kieffel et al. [16], to be considered a suitable option: high dielectric strength, good arc quenching capability, low boiling point, high vapor pressure at low temperature, high heat dissipation, and compatibility with the materials used in electrical switchgear, among others. Moreover, the gases must have low toxicity, no flammability, no ozone depletion potential (*ODP*), minimal environmental impact, and low *GWP*, to meet the environmental, health, and safety requirements.

The most important of these characteristics is the dielectric strength, or electric field strength (*E_{cr}*), which is defined as the maximum voltage that an insulating component can withstand before suffering electrical breakdown [17]. Currently, the different gases that are

being researched are hydrofluorocarbons (HFC), perfluorocarbons (PFC), fluoroketones (FK), fluoronitriles (FN), and hydrofluoroolefins (HFO) [15,16]. HFCs and PFCs have excellent dielectric properties [2], but their *GWP* is high, between 5000 and 12,000 in a 100-year horizon [16], making them not suitable environmentally. FKs and FNs have better dielectric properties than SF₆ [15]. One of the most researched FK, C₅F₁₀O, has almost the same *GWP* as CO₂, but its boiling point reaches 300 K. Although FNs have higher *GWP*, they present a lower boiling point, high stability, and material compatibility [18]. Finally, a certain researched HFO, C₃F₄H₂, has slightly lower dielectric strength than SF₆, a low boiling point, and low *GWP* [16].

Table 2 presents some of the gases and gas mixtures that have been researched for the replacement of SF₆ in medium and high voltage electrical switchgear, and their relative breakdown strength (*E_{rel}*), *GWP*, boiling temperature (*T_B*), lifetime (*LT*) in the atmosphere, toxicity threshold limit value–time weighted average (*TLV-TWA*), and decomposition products. The boiling temperature of all these gases is higher than the minimum operating temperature of outdoor medium voltage switchgear of 248 K, according to IEC 62271-200, except C₃F₈, so the gases must be diluted with a carrier gas to ensure that they do not liquefy in any circumstance. The most common carrier gases are the natural gases, CO₂, N₂, and dry air. The dielectric strength of the components is similar to that of SF₆, even after mixing them with the carrier gas, and the highest *GWP* is 70% lower. Besides, the lifetime in the atmosphere is lower than 20 days for the components CF₃I, C₃F₄H₂, C₅F₁₀O, and C₆F₁₂O. Furthermore, the *TLV-TWA* values of all the gas mixtures are lower than the one of SF₆; however, as they need to be mixed with a carrier gas, the toxicity decreases.

The key to identifying what could be a suitable alternative is to find a component with low *GWP* that preserves a high dielectric strength when it is diluted with a vector gas to reduce the boiling temperature. Various researchers have already presented patents for some of these gas mixtures for their use in medium and high voltage switchgear [19–22].

Table 2. Relative breakdown strength (*E_{rel}*), global warming potential values in a 100-year horizon (*GWP₁₀₀*), boiling point (*T_B*), toxicity threshold limit values–time weighted average (*TLV-TWA*), and decomposition products of the main researched alternative gas or gas mixtures to replace SF₆ in medium and high voltage switchgear.

Component	Mixture	<i>E_{rel}</i>	<i>GWP₁₀₀</i>	<i>T_B</i> (K)	<i>LT</i> (yr)	<i>TLV-TWA</i> (ppm _v)	Decomposition Products	Ref.
Sulfur hexafluoride (SF ₆)	Pure	1	23,500	209	3200	1000	COF ₂ , F ₂ , HF, H ₂ S, NF ₃ , F ₂ O, SO ₂ , S ₂ F ₁₀ , SF ₄ , SO ₂ F ₂	[1,23,24]
Trifluoroiodomethane (CF ₃ I)	Pure 30% CF ₃ I/CO ₂	1.2 0.8	<5	251	0.005	150	CF ₄ , C ₂ F ₆ , C ₂ F ₄ , C ₃ F ₈ , C ₃ F ₆ , C ₄ F ₈ , C ₂ F ₅ I, C ₃ F ₇ I, C ₂ F ₆ O ₃ , C ₃ F ₇ IO	[2,25–27]
Trifluoromethanesulphonyl fluoride (CF ₃ SO ₂ F)	Pure 50% CF ₃ SO ₂ F/N ₂	1.4 1	3678	251	40	*	No products after alternating current (AC) voltage breakdown	[28–30]
Octafluoropropane (C ₃ F ₈)	Pure 20% C ₃ F ₈ /N ₂	0.9 0.6	7000	236	2600			[31–33]
Heptafluorobutyronitrile (C ₄ F ₇ N)	Pure 5% C ₄ F ₇ N/N ₂ 20% C ₄ F ₇ N/CO ₂	2 0.9 1	2100	268	47	65	CF ₄ , C ₂ F ₆ , C ₃ F ₆ , C ₃ F ₈ , C ₂ F ₄ , F ₃ CC≡CCF ₃ , CF ₃ CF=CFCF ₃ , (CF ₃) ₃ CF, CF ₃ CN, C ₂ F ₅ CN, CNCN, HF, HCN, CO, CF ₃ CN, C ₂ F ₆	[34–37]
1,3,3,3-Tetrafluoropropene (C ₃ F ₄ H ₂)	Pure	0.8	6	254	0.05	1000	CF ₃ CCH, CF ₃ CCF, C ₂ H ₂ , C ₂ HF, CF ₄ , HF, CF ₃ H, C ₂ F ₆ , C ₂ F ₄ , C ₂ HF ₅ , CF ₃ HCF ₃ H, C ₃ F ₈	[23,38–40]
Heptafluoroisopropyl trifluoromethyl ketone (C ₅ F ₁₀ O)	Pure 5% C ₅ F ₁₀ O/Air	2 0.6	<1	300	0.04	225	CF ₄ , C ₂ F ₆ , C ₃ F ₈ , C ₃ F ₆ , C ₄ F ₁₀ , CF ₂ O	[15,41–44]
Perfluoro-2-methyl-3-pentanone (C ₆ F ₁₂ O)	Pure	2.7	<1	322	0.02	150		[15,41,45]

* Safety data sheet for CF₃SO₂F states that the component is fatal if swallowed, inhaled, or in contact with skin.

Binary and ternary mixtures made with the hydrofluoroolefin $C_3F_4H_2$, also known as HFO-1234ze(E), and the perfluoroketone $C_5F_{10}O$, have been studied. They will be referred to as HFO3E and PFK5, respectively, and their molecular structures are shown in Figure 1. These gases have been selected by Ormazabal Corporate Technology. Due to their boiling point being higher than that of SF_6 , as shown in Table 2, dry air has been used as a carrier gas. Because of that, the dielectric strength of the gas mixture is also reduced, so a balance must be found between getting the boiling point low enough, while maintaining the dielectric properties. The boiling point of PFK5 is higher than the one of HFO3E, which means that it should be more diluted. Moreover, this favors the fact that HFO3E has lower dielectric strength.

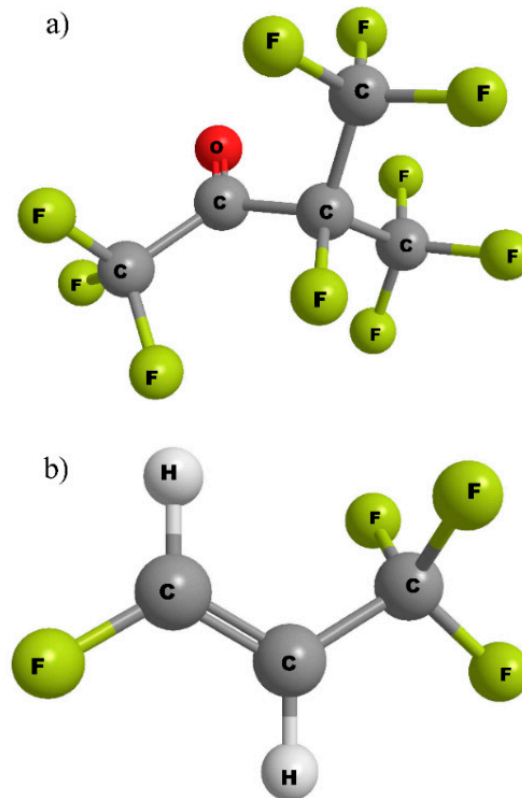


Figure 1. Molecular structures of (a) $C_5F_{10}O$ (PFK5) and (b) $C_3F_4H_2$ (HFO3E).

The understanding of the mixing process of these new gas mixtures is critical to define the physical and chemical properties that affect the electrical insulation and arc quenching properties. Therefore, the goal of this paper is the study of the diffusional behavior of the binary and ternary mixtures made with PFK5, HFO3E, and dry air, as possible alternatives for SF_6 for medium voltage switchgear, to anticipate the oncoming change of regulations. A chamber has been designed and built to study the diffusion of these binary and ternary mixtures, using UV-Vis spectroscopy to measure the concentration in the chamber during the mixing process. This technique was already used by some authors to measure these kinds of gases [46,47].

A diffusion process model is proposed to describe the mixture process; the model is fitted to the experimental concentration values in an algorithm developed in Scilab, which numerically calculates the diffusion parameters of the mixtures.

In this work, a novel experimental equipment capable of measuring and collecting the online concentration of a gas mixture has been designed and tested with fluorinated gas mixtures, candidates to replace SF_6 in medium voltage switchgear. Although this study has been focused on the analysis of a specific case of new fluorinated gas mixtures, this non-destructive technology would be of great interest for any application in which it is necessary to determine the physicochemical properties of a gas mixture through its

composition. Some examples include the design of gas mixtures that require specific characteristics, the monitoring of reactive mixtures, or the online malfunction detection and maintenance without the need to take samples that could compromise the integrity of the gas mixtures.

Moreover, a mathematical model that simulates the diffusion process of a component in a binary or ternary gas mixture has been proposed and implemented. The mixing process of the new insulating gas mixtures and the time it takes for them to reach stability have been determined.

This article intends to lay the groundwork for future experiments to study the effect of different perturbations, such as temperature, humidity, and concentration changes, among others, during the filling, mixing, and post-mixing process of the new insulating gas mixtures.

2. Materials and Methods

2.1. Experimental Equipment

The gas diffusion was determined using an experimental system that was specifically designed for this project to contain the gas mixtures and measure their concentration over time, using UV-Vis spectroscopy technology. The experimental equipment is shown in Figure 2.

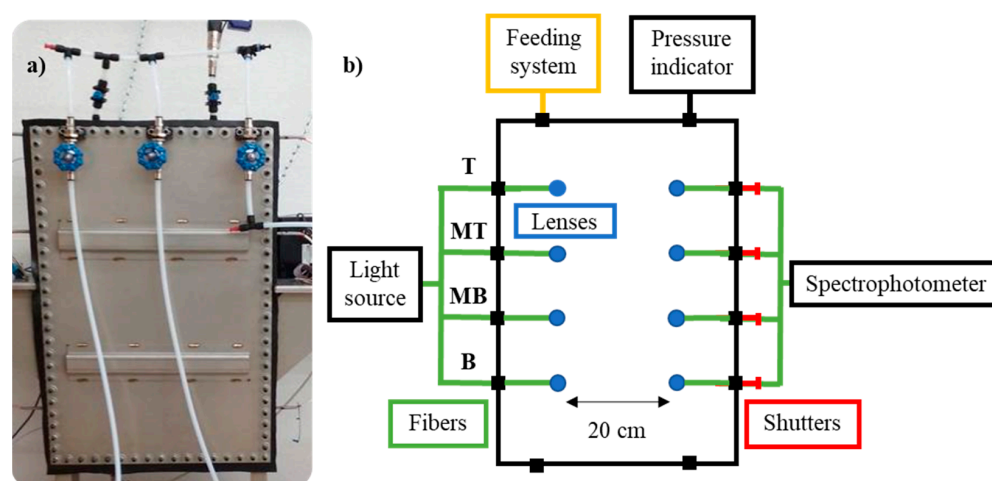


Figure 2. (a) Gas chamber and (b) scheme of the experimental equipment used for the gas diffusion study and its components. T (Top), MT (Medium Top), MB (Medium Bottom), and B (Bottom) correspond to the different heights of the measurement lines.

The designed system consisted of a 60 L tank, a DH-2000-S-DUV-TTL light source (Ocean Insight, Orlando, FL, USA), a Maya2000Pro spectrophotometer (Ocean Insight), a pressure indicator (WIKA, Klingenberg, Bayern, Deutschland), and a feeding system composed of polytetrafluoroethylene (PTFE) tubes to introduce the gas mixtures in the tank. The tank had similar dimensions to an actual medium voltage switchgear, but was slightly narrower, $0.8 \times 0.5 \times 0.15$ m, which favors vertical gas diffusion.

The light source emits a continuous UV-Vis spectrum, between 190–750 nm, which is split into the four fibers that end in four lenses that are located at four different heights of the tank, as the interest is focused on the diffusion that happens vertically. The measurement lines are located at 0.13, 0.35, 0.57, and 0.78 m; for simplicity reasons, the lines are referred to as Bottom (B), Medium Bottom (MB), Medium Top (MT), and Top (T), respectively.

The emitted light passes through the tank and is collected in four other lenses and fibers that merge and terminate in the spectrophotometer, which provides the corresponding ultraviolet absorbance spectra. A shutter is installed in each line, so the signal of each line is measured individually.

2.2. Mixing Process Tracking

The concentration (C) of the components in the gas mixtures that were studied are shown in Table 3. Each gas mixture was replicated three times. The components of the mixture were introduced in the tank one at a time through the feeding system, according to their molecular weight. An initial state of stratification by density was created by inserting the gases from heaviest to lightest, favoring the monitoring of the mixing process.

Table 3. Nomenclature and concentration (C) of the components of the studied gas mixtures.

Name	C_{PFK5} (%)	C_{HFO3E} (%)	C_{DRYAIR} (%)
B-10P	10	0	90
B-20P	20	0	80
B-40H	0	40	60
T-10P/40H	10	40	50

The dielectric strength, or critical field strength (E_{cr}), of the gas mixtures mentioned above can be estimated by a linear scaling according to Saxegaard et al. [48]:

$$E_{cr} = \sum_i^n x_i E_{cr,i} \left[\text{V m}^{-1} \text{Pa}^{-1} \right] \quad (1)$$

where x_i and $E_{cr,i}$ are the molar fraction and the electrical field strength of each component of the mixture, taking into consideration the dielectric strength of SF₆ and dry air (89 and 27 V m⁻¹ Pa⁻¹) [49], and the E_{rel} values of PFK5 and HFO3E that are shown on Table 2. The E_{cr} of components PFK5 and HFO3E are 178 and 71 V m⁻¹ Pa⁻¹, and the estimated values are 42, 57, 37, and 53 V m⁻¹ Pa⁻¹ for the gas mixtures B-10P, B-20P, B-40H, and T-10P/40H, respectively.

The measurement process of absorbance was automatized using LabVIEW, identifying the values of the absorbance for the 196 and 300 nm wavelengths, which correspond to the maximum absorption of HFO3E and PFK5, respectively. The system was programmed to open and close the shutters of the light source and the fibers, and to control the spectrophotometer to measure the reference intensities and calculate the absorbance of the four lines sequentially. The absorbance was calculated every 15 min for the first hour, every 20 min for the second hour, and every 30 min until the end of the experiment, which ends after 20 h.

Absorbance (A) was calculated by the Beer–Lambert Law [50]:

$$A = \log \left(\frac{I_0 - D_0}{I - D_0} \right) = \epsilon_M C l [\text{AU}] \quad (2)$$

where I_0 is the reference intensity, I is the intensity that is read after the absorption, and D_0 is the dark intensity, the one that the spectrophotometer reads when no light is emitted. A can also be expressed by the molar absorptivity (ϵ_M , m³ mol⁻¹ m⁻¹) multiplied by the molar concentration of the species (C) and the path length (l).

The mean value of the absorbance that is obtained in the three replicas of each experiment was the one used for the numerical calculation of the diffusion parameters.

2.2.1. Determination of the Concentration

The concentration was obtained through a calibration that relates it with the absorbance of each component. Four gas mixtures of known concentration were prepared for each component: 5%, 10%, 15% and 20% mixtures for PFK5, and 10%, 20%, 30% and 40% for HFO3E.

Each mixture was introduced in the gas chamber and the absorbance was monitored until the mixing process was completed, which means when all measurement lines displayed a similar value. The absorbance value that was obtained is the one related to the specific concentration that was introduced.

The A-C data were plotted and adjusted to linear regression to calculate the equations of the calibration curves. These equations allowed the calculation of the concentration of the components from the measurements of absorbance.

2.2.2. Diffusional Model

Two effects needed to be studied to determine the variation of concentration over time: (a) molecular diffusion, the transfer of individual molecules due to a concentration, pressure, or temperature gradient, among others; and (b) convection transport, caused by the overall movement of the fluid [51]. As the gases used in these experiments have high molecular weight, it was considered that the gas mixing process happened not only due to the concentration gradient, but also to the differences in the density of the components or natural convection.

Considering the described two effects, a modified Fick's generalized expression was obtained:

$$\frac{dC}{dt} = D \frac{\partial^2 C_i}{\partial z^2} + \frac{\partial(V_i C_i)}{\partial z} \quad (3)$$

where C_i is the concentration, D ($\text{m}^2 \text{s}^{-1}$) is the diffusion coefficient, t represents the time, and z the height. V_i is the velocity caused by the differences between densities:

$$V_i = K (\rho_m - \rho_i) [\text{m s}^{-1}] \quad (4)$$

where K ($\text{m}^4 \text{kg}^{-1} \text{s}^{-1}$) is the convection constant. The density of the heavy component in the binary mixture (ρ_m) and the density of the mixture at each point in time (ρ_i) were calculated by:

$$\rho_m = \frac{P MW_m}{R T} [\text{kg m}^{-3}] \quad (5)$$

$$\rho_i = \frac{P MW_i}{R T} [\text{kg m}^{-3}] \quad (6)$$

T and P are the temperature and pressure at which the experiments were carried out, 298 K and 1 atm (101,325 Pa), and R is the ideal gas constant. MW_m is the molecular weight of the heavy component of the binary mixture, and MW_i indicates the molecular weight of the mixture at each point in time, which was calculated by the weighted average of the MW_m of each component of the mixture:

$$MW_i = \sum_c^n y_m MW_m [\text{kg mol}^{-1}] \quad (7)$$

The equations were based on the fact that for a binary mixture consisting of components A and B, the diffusivity of A in B (D_{AB}), and vice versa (D_{BA}), are the same [51]. Both molecular diffusion and natural convection were considered to determine the molar flux (J):

$$J = -D \frac{dC_i}{dz} + V_i C_i [\text{mol m}^{-2} \text{s}^{-1}] \quad (8)$$

Theoretical studies of multicomponent diffusion are based on the Stefan–Maxwell equation, which, in turn, was derived from the solution of the Boltzmann equation [52]. For isothermal and isobaric conditions, this equation is a strong approximation that satisfies the practical requirement. The variation of concentration over time for multicomponent mixtures is represented in the following equation:

$$\left(\frac{dC}{dt}\right) = [D] \left(\frac{\partial^2 C_i}{\partial z^2}\right) + \left(\frac{\partial(V_i C_i)}{\partial z}\right) \quad (9)$$

The element $[D]$ is a size $n - 1$ squared matrix that represents the diffusion coefficients, n being the number of components in the mixture. The elements of the square matrix $[D]$

are called practical diffusion coefficients [52]. In this study, a gas mixture composed of three elements was made; therefore, the matrix was composed of 2×2 elements. As well as in binary gas mixtures, the convection effect was also considered in multicomponent mixing:

$$\begin{pmatrix} \frac{dC_1}{dt} \\ \frac{dC_2}{dt} \end{pmatrix} = \begin{bmatrix} D_{11} & D_{12} \\ D_{21} & D_{22} \end{bmatrix} \begin{pmatrix} \frac{\partial^2 C_1}{\partial z^2} \\ \frac{\partial^2 C_2}{\partial z^2} \end{pmatrix} + \begin{pmatrix} \frac{\partial(V_1 C_1)}{\partial z} \\ \frac{\partial(V_2 C_2)}{\partial z} \end{pmatrix} \quad (10)$$

Hence, the concentration differential of each component over time depends on the practical diffusion coefficients of both components and their concentration differential over the position in the gas chamber [52]:

$$\frac{dC_1}{dt} = D_{11} \frac{\partial^2 C_1}{\partial z^2} + D_{12} \frac{\partial^2 C_2}{\partial z^2} + \frac{\partial(V_1 C_1)}{\partial z} \quad (11)$$

$$\frac{dC_2}{dt} = D_{21} \frac{\partial^2 C_1}{\partial z^2} + D_{22} \frac{\partial^2 C_2}{\partial z^2} + \frac{\partial(V_2 C_2)}{\partial z} \quad (12)$$

Furthermore, the effective diffusivity coefficients (D_{eff}) were calculated using the practical diffusion coefficients [52]. Bird et al. [53] stated that the molar fraction gradients could be replaced by molar fraction differences to simplify the calculations:

$$D_{1,eff} = \sum_{k=1}^{n-1} D_{1k} \frac{\nabla y_k}{\nabla y_1} [\text{m}^2 \text{ s}^{-1}] \quad (13)$$

Furthermore, according to Taylor and Krishna [52], the diffusivity eigenvalues of the components (\hat{D}_1 and \hat{D}_2) must be positive:

$$\hat{D}_1 = \frac{1}{2} \left(\text{tr}[D] + \sqrt{\text{disc}[D]} \right) \quad (14)$$

$$\hat{D}_2 = \frac{1}{2} \left(\text{tr}[D] - \sqrt{\text{disc}[D]} \right) \quad (15)$$

where $\text{tr}[D]$ is the trace and $\text{disc}[D]$ is the discriminant of the matrix. Because of Equations (14) and (15), the conditions presented in the following equations must be met:

$$D_{11} + D_{22} > 0 \quad (16)$$

$$D_{11} D_{22} - D_{12} D_{21} > 0 \quad (17)$$

$$(D_{11} - D_{22})^2 + 4 D_{12} D_{21} > 0 \quad (18)$$

The proposed mathematical model was reproduced in an algorithm created in Scilab. The purpose of the program is the numerical calculation of the differential Equations (3), (11) and (12) to obtain the optimized diffusion and convection coefficients by minimizing an error objective function (OF):

$$\text{OF} = \frac{\sum_1^{4N} (C_{exp} - C_{model})^2}{4N} \quad (19)$$

Such OF was defined as the sum of the squared differences between the experimental values of the concentration (C_{exp}) and the ones obtained in the model (C_{model}) divided by the whole amount of measured concentrations in the lines (N). The relative standard error (RSE) [54] between the experimental concentration values and the model was also calculated by referencing them to the final concentration value (C_{final}):

$$\text{RSE} = \sqrt{\frac{\sum_1^{4N} \left(\frac{C_{exp} - C_{model}}{C_{final}} \right)^2}{4N - 1}} 100 [\%] \quad (20)$$

The optimization algorithm looked for the values of D and K in the differential equations so that the theoretical model fitted the experimental values and also calculated the relative standard error.

Additionally, the binary diffusion coefficients (D_E) were also calculated using the correlation proposed by Fuller, Schettler, and Giddings [52,55]:

$$D_E = D_{AB} = 0.01883 T^{1.75} \frac{\sqrt{\frac{M_A + M_B}{M_A M_B}}}{P [\sqrt[3]{\sum v_A} + \sqrt[3]{\sum v_B}]^2} \left[\text{m}^2 \text{s}^{-1} \right] \quad (21)$$

The results were compared with the numerically obtained optimized diffusion constants of all binary mixtures. The binary diffusion coefficient between components A and B (D_{AB}) depends on the temperature (T , K), pressure (P , Pa), molecular weight (M , g mol^{-1}), and atomic diffusion volumes (v). The values of v for the atoms C, H, O, and F are 15.9, 2.31, 6.11, and 14.7, respectively [56].

The values of D_E of the ternary mixture were calculated by dividing the mixture into two pseudo-binary mixtures between one heavy component against the other two components as a whole. The estimated value for each heavy component was compared with the numerically calculated D_{eff} values.

3. Results and Discussion

3.1. Mixing Process Tracking

3.1.1. Determination of the Concentration

The calibration curve of each component and measurement line is shown in Figure 3. The curves present a linear tendency. The linear regression equations, correlation coefficients (r^2), and the molar absorptivity of PFK5 and HFO3E were calculated, and they are collected in Table 4. The results show that the sensitivity of the measuring system for HFO3E is considerably lower than the one of PFK5, due to the great difference in the molar absorptivity of both gases.

The maximum absorption of the component HFO3E is located at 196 nm in the UV-Vis spectrum, where it is common to find noise when measuring the absorbance since this wavelength shows very poor selectivity. Because of this, the concentration, velocity and molar flux profiles of HFO3E have more deviations and are less accurate.

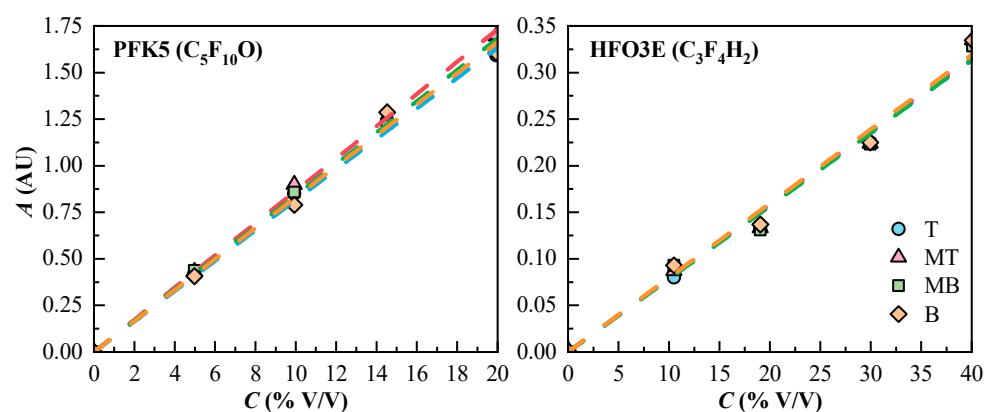


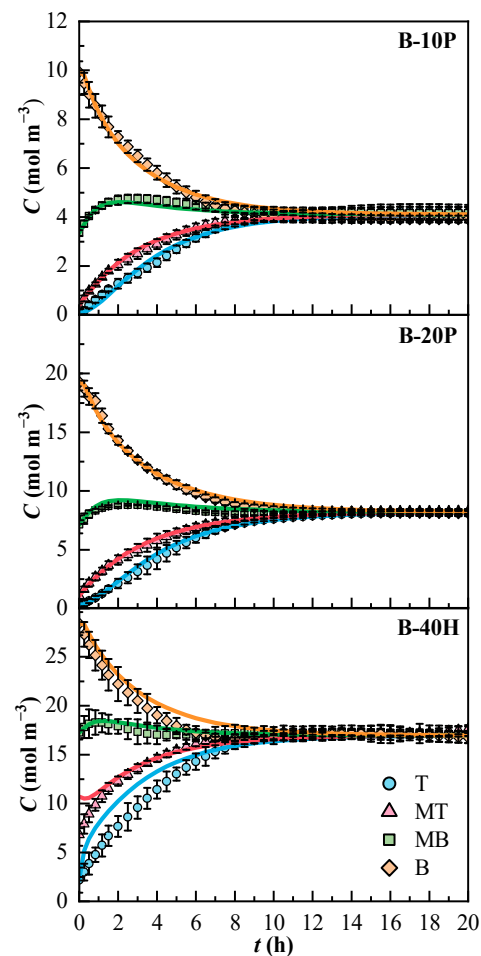
Figure 3. Experimental concentration values (C_{exp} , dots) and calibration curves (dashed lines) of the components of the gas mixtures. T (Top, \circ), MT (Medium Top, \triangle), MB (Medium Bottom, \square), and B (Bottom, \diamond) correspond to the different heights of the measurement lines.

Table 4. Linear regression equations, correlation coefficients (r^2), and molar absorptivities (ϵ_M), of PFK5 and HFO3E.

	Line	Linear Regression	r^2	ϵ_M ($\text{m}^3 \text{mol}^{-1} \text{cm}^{-1}$)
PFK5	T	$y = 0.0811x$	0.997	9.9
	MT	$y = 0.0852x$	0.999	10.4
	MB	$y = 0.0827x$	0.999	10.1
	B	$y = 0.0826x$	0.994	10.1
HFO3E	T	$y = 0.0081x$	0.991	0.99
	MT	$y = 0.0081x$	0.989	0.99
	MB	$y = 0.0079x$	0.988	0.97
	B	$y = 0.0081x$	0.989	0.98

3.1.2. Diffusional Model

The concentration profiles of the model and the diffusional coefficients were obtained thanks to the optimization process in Scilab. The concentration profiles of the binary mixtures are plotted in Figure 4. The 95% confidence interval of the experimental values is indicated. The B-40H mixture showed broader confidence intervals than the binary mixtures of PFK5. The concentration of all binary mixtures reached stabilization after 10 h. The molar concentrations at the end of the experiments were 4.1 and 8.2 mol m^{-3} for the PFK5 mixtures and 17.1 mol m^{-3} for the HFO3E mixture.

**Figure 4.** Experimental (C_{exp} , dots) and estimated (C_{model} , solid lines) concentration profiles of the binary mixtures over time. T (Top, \circ), MT (Medium Top, \triangle), MB (Medium Bottom, \square), and B (Bottom, \diamond) correspond to the different heights of the measurement lines.

The model fitted the experimental data of B-10P and B-20P mixtures correctly. The concentration profiles from the mixture B-40H show that the model deviated in lines T and B at the beginning of the experiment. The molar absorptivity of HFO3E is ten times lower than that of PFK5 in the UV spectrum. T is the line that shows the lowest concentration and B is the line that shows the highest molar flux, as will be discussed later.

The concentration profiles obtained for the T-10P/40H mixture are shown in Figure 5. In general, the ternary mixture showed greater confidence intervals than the binary mixtures. Line MB exhibited less variation in both components than the others. Even though the whole mixture stabilized after 12 h, the concentration of HFO3E was stable after 10 h. The compound PFK5 is the one that determines the duration of the mixing process, as it is the one with the lower effective diffusion coefficient. The molar concentrations at the end of the experiments were 4.4 mol m^{-3} for PFK5 and 16.6 mol m^{-3} for HFO3E. The model fitted the experimental data correctly, although the concentration profile of HFO3E also deviated from the confidence interval in lines T and B, like in mixture B-40H.

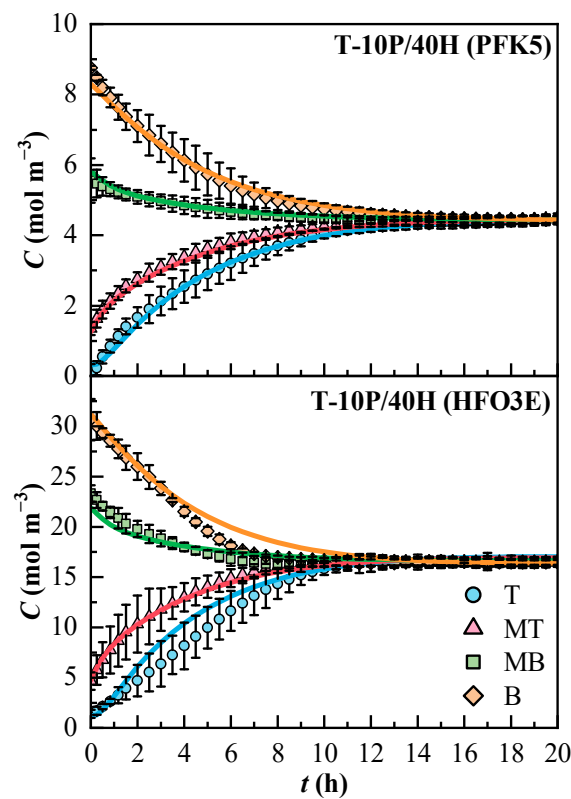


Figure 5. Experimental (C_{exp} , dots) and estimated (C_{model} , solid lines) concentration profiles of the components of the ternary mixture over time. T (Top, \circ), MT (Medium Top, \triangle), MB (Medium Bottom, \square), and B (Bottom, \diamond) correspond to the different heights of the measurement lines.

The optimized diffusion and convective coefficients, the theoretically estimated coefficients, and relative standard error for the binary mixtures are shown in Table 5. As diffusion does not depend on concentration, the D of mixtures B-10P and B-20P should be equal, and they are similar. Additionally, the K values are very low. It can be assumed that the convection mechanism had little effect on the mixing process. The RSE for all binary mixtures is lower than 6%, and the mixture whose model best fitted the experimental data was B-20P, which also has the lowest diffusion coefficient. The optimized coefficients of the PFK5 mixtures are more similar to the estimated one than the HFO3E mixture, and the error increases with the concentration.

Table 5. Diffusion (D_E and D) and convective (K) coefficients and relative standard error (RSE) of the binary mixtures after the optimization process using Scilab.

Mixture	D_E * ($\text{m}^2 \text{s}^{-1}$)· 10^6	D ($\text{m}^2 \text{s}^{-1}$)· 10^6	K ($\text{m}^4 \text{kg}^{-1} \text{s}^{-1}$)· 10^{14}	RSE (%)
B-10P	5.4	5.2	3.1	3.8
B-20P	5.4	4.8	2.7	2.6
B-40H	7.9	5.3	2.7	5.3

* Theoretically estimated using Equation (21).

For the ternary mixture, the values of the practical diffusion coefficients were the following:

$$[D] = \begin{pmatrix} D_{11} & D_{12} \\ D_{21} & D_{22} \end{pmatrix} = \begin{pmatrix} 0.0195 & -0.0017 \\ 0.0535 & 0.0001 \end{pmatrix} \quad (22)$$

The conditions that Taylor and Krisna described [52], which are shown in Equations (16)–(18), were met.

The diffusion and convection coefficients and RSE values are shown in Table 6. Both values of K are also very low in the ternary mixture. The D_{eff} for PFK5 and HFO3E are calculated from Equation (13). They are lower than the D obtained for the binary mixtures, which states that the ternary mixture diffuses slower than the binary mixtures. The D_{eff} for HFO3E is higher than the D_{eff} for PFK5. That of HFO3E is closer to its estimated value than the one of PFK5. HFO3E diffuses slower and PFK5 diffuses faster than what was theoretically estimated. Overall, the model fitted better the experimental data of PFK5 than the data of HFO3E. The results are consistent with what is shown in Figure 5.

Table 6. Diffusion ($D_{eff,E}$ and D_{eff}) and convective (K) coefficients and relative standard error (RSE) of the components of the ternary mixture after the optimization process in Scilab.

Component	$D_{eff,E}$ * ($\text{m}^2 \text{s}^{-1}$)· 10^6	D_{eff} ($\text{m}^2 \text{s}^{-1}$)· 10^6	K ($\text{m}^4 \text{kg}^{-1} \text{s}^{-1}$)· 10^{11}	RSE (%)
PFK5	2.9	3.6	0.6	2.2
HFO3E	4.4	3.9	2.2	4.4

* Theoretically estimated using Equation (21).

The convection velocity of the binary mixtures is shown in Figure 6. The velocity is negative, as K is positive and the mixture with air has lower density than PFK5 or HFO3E. The convection phenomenon pushes down the heavy components of the mixtures. The most negative velocity values are found in line T, which is the highest line in the gas chamber and therefore the most affected by the high density of the components. The velocities are less negative as the height in which the measurement line is located decreases. Nonetheless, the convection velocity is so small that it is almost negligible.

The convection velocity of T-10P/40H is shown in Figure 7. As the component PFK5 is the heaviest, its convection velocity is always negative, because any mixture between HFO3E and air will always have lower density than PFK5. The convection velocity of component HFO3E is positive in line B at the beginning of the experiment, which happens because the higher concentration of PFK5 pushes up HFO3E and the carrier gas.

The molar flux of the binary mixtures is shown in Figure 8. All binary mixtures have a similar tendency. The molar flow is higher in line B, the one that presents the highest concentration values. The molar flow is almost zero in line T. The molar flow of lines MT and MB slightly increase at the beginning of the experiments.

The molar flux of the ternary mixture can be observed in Figure 9. Both molar flux profiles share the same tendency, are very similar, and reach zero approximately at the same time. The lines that present higher molar flux are MT and MB, as they show the highest concentration gradients between all components. The molar flux of line B is the one that increased at the beginning of the mixing process, and line T is also almost zero.

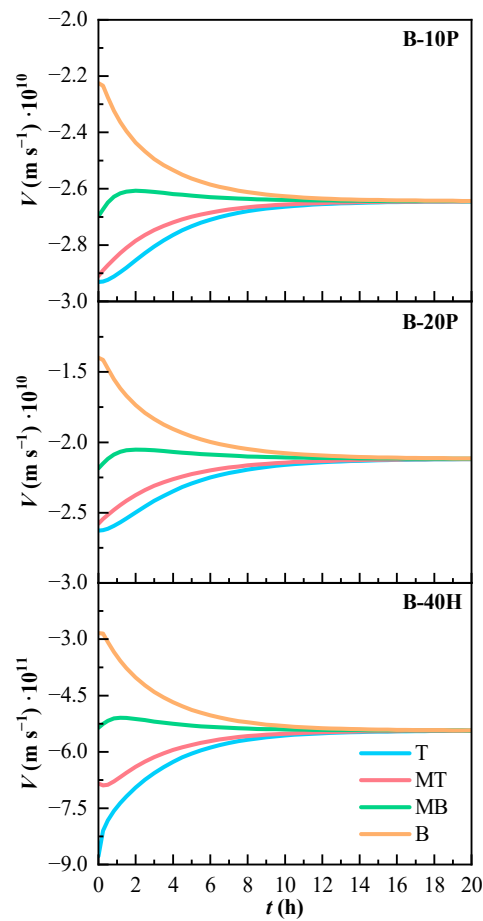


Figure 6. Variation of the estimated convection velocity (V) of the binary mixtures over time. T (Top), MT (Medium Top), MB (Medium Bottom), and B (Bottom) correspond to the different heights of the measurement lines.

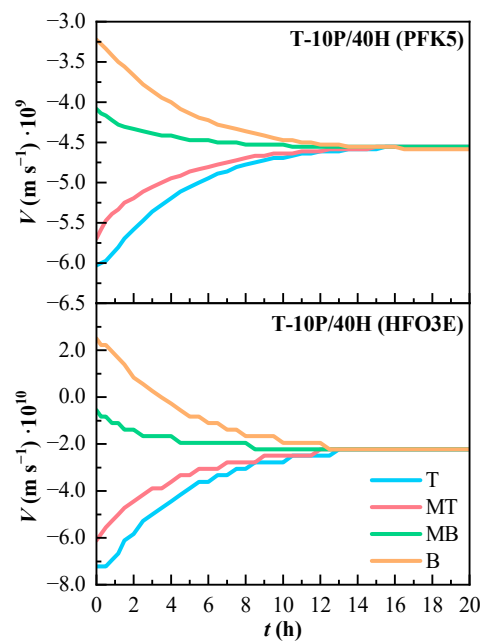


Figure 7. Variation of the estimated convection velocity (V) of the components of the ternary mixture over time. T (Top), MT (Medium Top), MB (Medium Bottom), and B (Bottom) correspond to the different heights of the measurement lines.

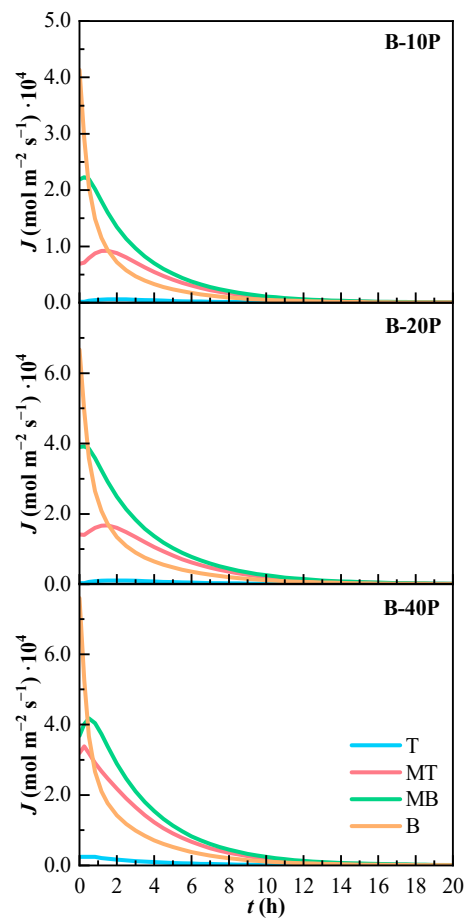


Figure 8. Variation of the estimated molar flux (J) of the binary mixtures over time. T (Top), MT (Medium Top), MB (Medium Bottom), and B (Bottom) correspond to the different heights of the measurement lines.

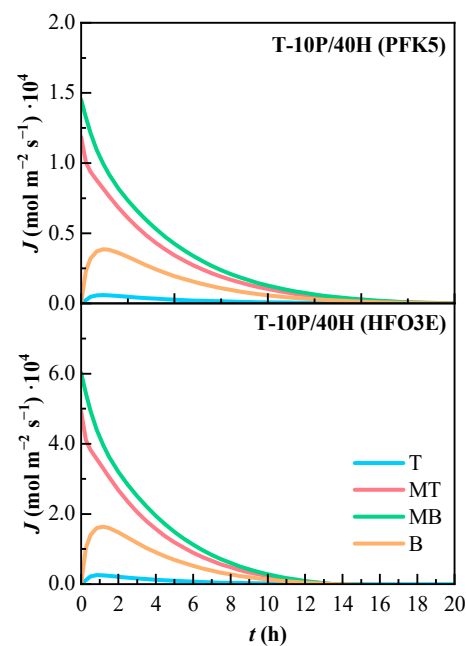


Figure 9. Variation of the estimated molar flux (J) of the components of the ternary mixture over time. T (Top), MT (Medium Top), MB (Medium Bottom), and B (Bottom) correspond to the different heights of the measurement lines.

The molar flux profiles, together with the obtained concentration and velocity profiles, represent that all the mixtures reached homogeneity and stability at the end of the experiments.

3.1.3. Model Validation

The validation of the model was carried out to determine its accuracy not only for the gas mixtures used to build it, but also for mixtures made with other concentration values too [53]. Five gas mixtures were proposed, different from the ones used to prepare the model. The composition of the gas mixtures is shown in Table 7.

Table 7. Nomenclature and concentration (C) of the components of the gas mixtures used for validation.

Name	C_{PFK5} (%)	C_{HFO3E} (%)	C_{DRYAIR} (%)
B-5P	5	0	95
B-15P	15	0	85
B-15H	0	15	85
B-30H	0	30	70
T-20P/40H	20	40	50

The concentration profiles of these mixtures were simulated. The D and K coefficients that were used for the binary mixtures are the ones shown in Table 5, and the D_{eff} and K coefficients that were used for the ternary mixture are obtained from Table 6. The residuals of each mixture, throughout the whole experiment, were calculated:

$$Residual = C_{exp} - C_{model} \left[\text{mol m}^{-3} \right] \quad (23)$$

The mean residual value of all four measurement lines at a specific time (\overline{R}_t) and the mean residual value of a specific measurement line (\overline{R}_L) until the end of the experiment (t_f) were also calculated:

$$\overline{R}_t = \frac{\sum_{L=1}^4 (C_{exp} - C_{model})_L}{4} \left[\text{mol m}^{-3} \right] \quad (24)$$

$$\overline{R}_L = \frac{\sum_{t=0}^{t_f} (C_{exp} - C_{model})_t}{N} \left[\text{mol m}^{-3} \right] \quad (25)$$

The end of the experiment was considered when the concentration of the four lines reached stabilization. All the mean residual values were represented against C_{exp} , including the mixtures that were used for building the model [53]. \overline{R}_t is represented against C_{exp} in Figure 10. The residuals of PFK5 do not show a distinct tendency; they are distributed almost evenly in the positive and negative sides of the y -axis and are near zero. This shows that the error of PFK5 is not carried over with the model. There is no significant difference between the \overline{R}_t of PFK5 of binary and ternary mixtures.

The results for HFO3E show higher residual values and they are not evenly distributed. Most of them are negative values, which shows that the model is more likely to present higher values than the experimental ones. The residuals also decrease with time, so the model showed better results near stabilization. The low absorptivity of this component, together with the higher molar flow at the beginning of the experiments, makes it more difficult to predict the values of concentration. Besides, the concentration of HFO3E of the binary mixtures is easier to calculate as the residuals are lower.

\overline{R}_L is represented against C_{exp} in Figure 11. Lines T and MB show lower residual values for both components. PFK5 clearly shows lower residual values in both binary and ternary mixtures. The values of HFO3E of the ternary mixtures are higher than the ones of the binary mixtures. The model will predict lower values than the experimental ones in line MT and higher ones in line B. Line B shows the highest absolute residual values, especially for HFO3E. The higher molar concentration and molar flux that was found in this line complicated the ability of the model to predict the concentration values.

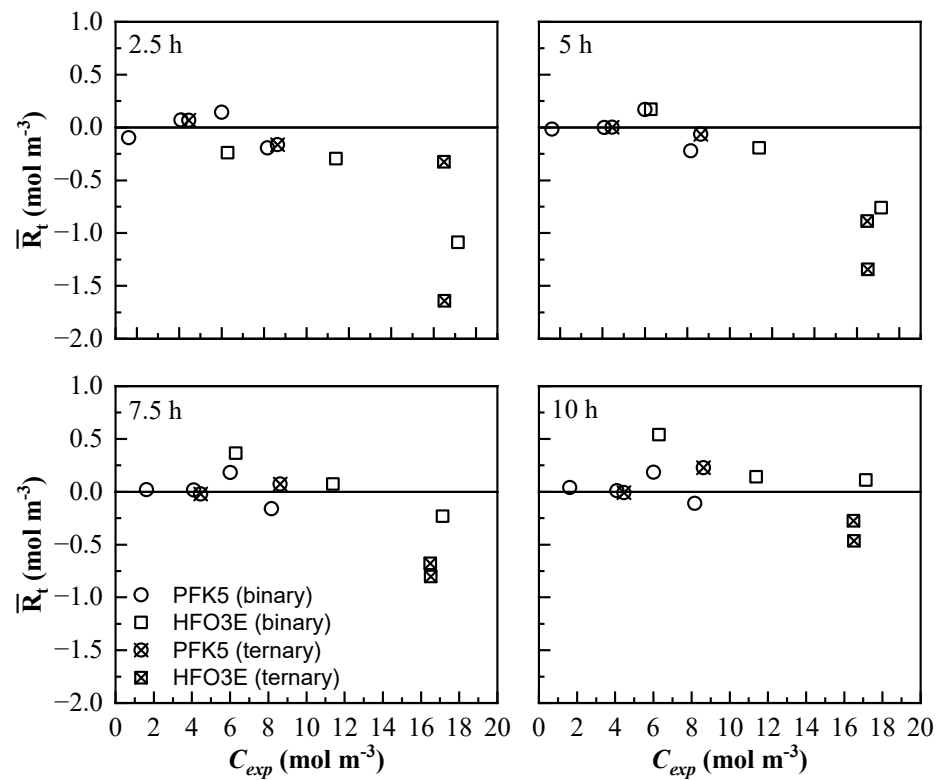


Figure 10. Mean residual value of all measurement lines at different times (\bar{R}_t) of the mixing process. The results of all the binary (\circ and \square) and ternary (\otimes and \boxtimes) mixtures are represented for PFK5 and HFO3E, respectively.

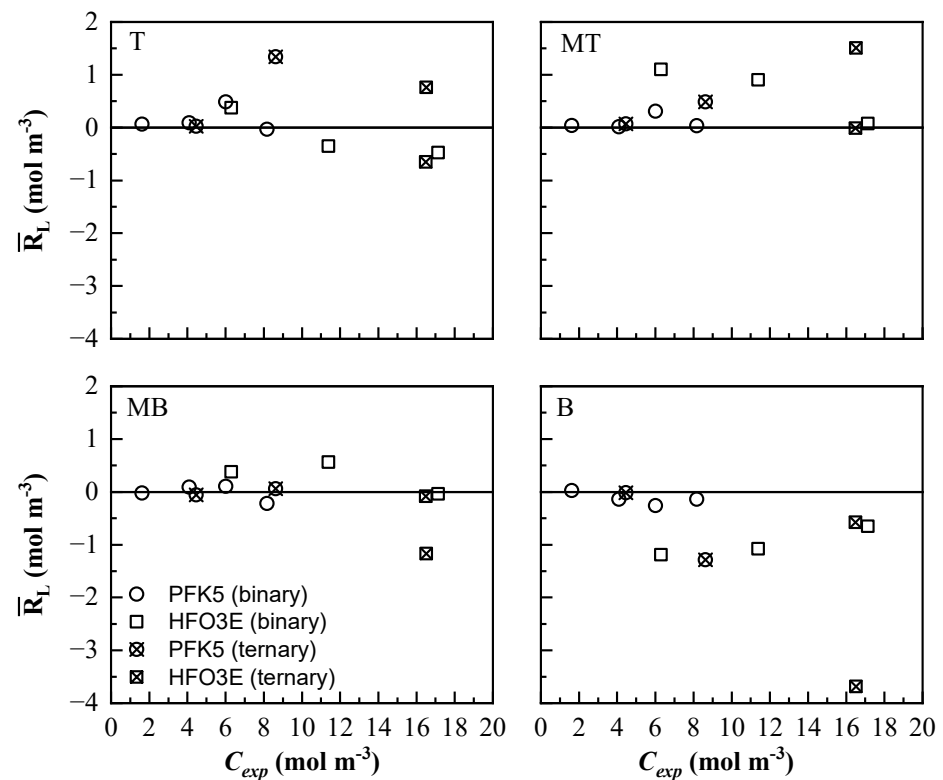


Figure 11. Mean residual value of the measurement lines at all times (\bar{R}_L) of the mixing process. The results of all the binary (\circ and \square) and ternary (\otimes and \boxtimes) mixtures are represented for PFK5 and HFO3E, respectively.

The minimum and maximum absolute residual values for all mixtures are shown in Table 8. As all gas mixtures reach stability after 10 h, only results before that were considered. The maximum residual values of PFK5 were found in line B at the beginning of the experiments. The minimum ones were distributed into all lines.

Table 8. Minimum and maximum absolute residual values of the mixtures.

Mixture	Minimum Absolute Residuals			Maximum Absolute Residuals			
	Value·10 ³ (mol m ⁻³)	t (h)	Line	Value (mol m ⁻³)	t (h)	Line	
PFK5	B-10P	9	0.5	MT	0.34	0.5	B
	B-20P	0.83	1.5	T	0.73	1	B
	T-10P/40H	2	8	T	0.34	0.5	B
	B-5P	0.33	5.5	B	0.28	2.5	T
	B-15P	3	2.5	MB	1.88	0.5	B
	T-20P/40H	3.4	8.5	MB	4.09	0.5	B
HFO3E	B-40H	2.4	8	MB	2.73	1	T
	T-10P/40H	20	10	T	2.25	3.5	T
	B-15H	40	7.5	T	3.57	2.5	B
	B-30H	300	10	MB	3.51	3	B
	T-20P/40H	450	10	T	7.39	3.5	B

HFO3E showed its maximum residuals distributed between lines T and B at the beginning of the experiments. The minimum residual values of HFO3E increase when the concentration increases. The T-20P/40H mixture was the one that showed the highest maximum absolute residuals, which were presented in line B.

4. Conclusions

A novel piece of experimental equipment has been designed, and an automatized measurement system, which has been programmed in LabVIEW, has been implemented for the online monitoring of the mixing process of the gas mixtures.

Consequently, it has been possible to determine the duration of the mixing process of new insulating gas mixtures made of PFK5 and HFO3E, candidates to replace SF₆ in MVS. Starting from an initial stratification state caused by the feeding of the gases depending on their molecular weight, stability in the mixtures has been reached between 10 and 12 h, depending on the composition of the mixture. Besides, binary mixtures have reached stability before the ternary mixture. In addition, it has been seen that the molar absorptivity of HFO3E is lower than of PFK5, and that it absorbs at 196 nm in the UV-Vis spectrum, which has hindered measurements.

A mathematical model that describes the mixing process has been proposed, which takes both natural convection and molecular diffusion into consideration. The model has made it possible to obtain the diffusion and convection coefficients of the mixtures with a relative standard error lower than 6%. In comparison with the calculation of the diffusion coefficient of HFO3E that Hu et al. [57] performed, the estimation shares the same order of magnitude, although it is slightly higher in this work. The convection coefficients of all the mixtures have been significantly low, which could prove that the effect of natural convection is negligible in comparison with molecular diffusion of the order of 10⁵ (in the ternary mixture) to 10⁸ (in the binary mixtures) times smaller.

The residuals of PFK5, which have shown no significant tendency, neither in sign (positive or negative) nor in value, are lower than 1.9 mol m⁻³ for the binary mixtures and 4.1 for the ternary mixtures. Those of HFO3E have been higher at the beginning of the experiment, between 2.3 and 7.4 mol m⁻³, and have decreased with time, reaching values as low as 2.4 × 10⁻³ mol m⁻³. The model has predicted the concentration values of line MB, for example, better than that of the bottom line, probably due to high variability in the concentration.

It has been possible to predict the concentration profiles of a mixing process of gas mixtures made of PFK5 to be better than the ones made of HFO3E, using air as the carrier gas. The low absorptivity of HFO3E in the UV spectrum has led to higher residual values in the lines that have the highest and lowest concentration of both binary and ternary mixtures. This indicates that UV-Vis could not be the best technique to monitor the concentration changes of this component.

Through this work, the physical characterization of the diffusion process and mixing stability of binary and ternary gas mixtures made of PFK5 and HFO3E was started. All this information is postulated as a methodological and diffusional modeling basis for future studies that take into account other disturbances, such as temperature, humidity, and electrical discharge, among others. Nevertheless, attention also needs to be paid to the chemical stability of the mixtures using analytical methods in future studies.

Author Contributions: Conceptualization, J.I.L.; methodology, A.E. and L.C.; software, E.A., A.E. and B.P.-A.; validation, A.E., M.L.A. and R.M.A.; formal analysis, A.E.; investigation, A.E. and L.C.; resources, J.I. (Jesús Izcara) and J.I. (Josu Izagirre); data curation, A.E.; writing—original draft preparation, A.E. and L.C.; writing—review and editing, J.I.L., M.L.A. and R.M.A.; visualization, J.I.L.; supervision, J.I.L.; project administration, J.I.L., R.M.A. and J.I. (Josu Izagirre); funding acquisition, J.I.L., R.M.A. and J.I. (Josu Izagirre). All authors have read and agreed to the published version of the manuscript.

Funding: This research was funded by the Basque Government, grant numbers KK-2017/00090 and KK-2019/00017.

Institutional Review Board Statement: Not applicable.

Informed Consent Statement: Not applicable.

Data Availability Statement: Not applicable.

Conflicts of Interest: The authors declare no conflict of interest.

References

1. Tsai, W.-T. The decomposition products of sulfur hexafluoride (SF₆): Reviews of environmental and health risk analysis. *J. Fluor. Chem.* **2007**, *128*, 1345–1352. [CrossRef]
2. Xiao, S.; Zhang, X.; Tang, J.; Liu, S. A review on SF₆ substitute gases and research status on CF₃I gases. *Energy Rep.* **2018**, *4*, 486–496. [CrossRef]
3. Stocker, T.F.; Qin, D.; Plattner, G.-K.; Tignor, M.M.B.; Allen, S.K.; Boschung, J. Climate Change 2013: The Physical Science Basis. Intergovernmental Panel on Climate Change. 2013. Available online: <https://www.ipcc.ch/report/ar5/wg1/> (accessed on 13 December 2021).
4. United Nations. Kyoto Protocol to the United Nations Framework Convention on Climate Change. 1998. Available online: https://unfccc.int/kyoto_protocol (accessed on 14 December 2021).
5. Hyrenbach, M.; Paul, T.A.; Owens, J. Environmental and safety aspects of AirPlus insulated GIS. In Proceedings of the 24th International Conference & Exhibition on Electricity Distribution, Glasgow, UK, 12–15 June 2017.
6. Weiss, R.F.; Mühle, J.; Salameh, P.K.; Harth, C.M. Nitrogen trifluoride in the global atmosphere. *Geophys. Res. Lett.* **2008**, *35*, L20821. [CrossRef]
7. Morais, A.R.C.; Harders, A.N.; Baca, K.R.; Olsen, G.M.; Befort, B.J.; Dowling, A.W.; Maginn, E.J.; Shiflett, M.B. Phase Equilibria, Diffusivities, and Equation of State Modeling of HFC-32 and HFC-125 in Imidazolium-Based Ionic Liquids for the Separation of R-410A. *Ind. Eng. Chem. Res.* **2020**, *59*, 18222–18235. [CrossRef]
8. Mühle, J.; Ganesan, A.L.; Miller, B.R.; Salameh, P.K.; Harth, C.M.; Grealley, B.R.; Rigby, M.; Porter, L.W.; Steele, L.P.; Trudinger, C.M.; et al. Perfluorocarbons in the global atmosphere: Tetrafluoromethane, hexafluoroethane, and octafluoropropane. *Atmos. Chem. Phys.* **2010**, *10*, 5145–5164. [CrossRef]
9. Corr, S. 1,1,1,2-Tetrafluoroethane; from refrigerant and propellant to solvent. *J. Fluor. Chem.* **2002**, *118*, 55–67. [CrossRef]
10. Akasaka, R.; Zhou, Y.; Lemmon, E.W. A Fundamental Equation of State for 1,1,1,3,3-Pentafluoropropane (R-245fa). *J. Phys. Chem. Ref. Data* **2015**, *44*, 013104. [CrossRef]
11. The European Parliament and the Council of the European Union. Regulation (EU) No 517/2014 of the European Parliament and of the Council of 16 April 2014 on Fluorinated Greenhouse Gases and Repealing Regulation (EC) No 842/2006. 2014, 150/195-230. Available online: <https://eur-lex.europa.eu/eli/reg/2014/517/oj> (accessed on 14 December 2021).
12. European Commission. Climate Action: EU Legislation to Control F-Gases. Available online: https://ec.europa.eu/clima/policies/f-gas/legislation_en (accessed on 14 December 2021).

13. Nagarsheth, R.; Singh, S. Study of gas insulated substation and its comparison with air insulated substation. *Int. J. Electr. Power Energy Syst.* **2014**, *55*, 481–485. [[CrossRef](#)]
14. Sato, J.; Sakaguchi, O.; Kubota, N.; Makishima, S.; Kinoshita, S.; Shioiri, T.; Yoshida, T.; Miyagawa, M.; Homma, M.; Kaneko, E. New technology for medium voltage solid insulated switchgear. In Proceedings of the IEEE Transmission and Distribution Conference and Exhibition, Yokohama, Japan, 6–10 October 2002.
15. Hyrenbach, M.; Zache, S. Alternative insulation gas for medium-voltage switchgear. In Proceedings of the 2016 Petroleum and Chemical Industry Conference Europe, Berlin, Germany, 14–16 June 2016.
16. Kieffel, Y.; Irwin, T.; Ponchon, P.; Owens, J. Green Gas to Replace SF₆ in Electrical Grids. *IEEE Power Energy Mag.* **2016**, *14*, 32–39. [[CrossRef](#)]
17. Pionteck, J.; Wypych, G. *Handbook of Antistatics*, 2nd ed.; ChemTech Publishing: Toronto, ON, Canada, 2016.
18. Kieffel, Y.; Biquez, F. SF₆ alternative development for high voltage switchgears. In Proceedings of the 2015 IEEE Electrical Insulation Conference, Seattle, WA, USA, 7–10 June 2015.
19. Izcara, J.; Larrieta, J. Electrical Insulation System for Medium- and High-voltage Electrical Switchgear. U.S. Patent 10,607,748 B2, 31 March 2020.
20. Glasmacher, P. Fluorinated Ketones as a High-Voltage Insulating Medium. WO Patent 2010/146022A1, 23 December 2010.
21. Mantilla, J.; Claessens, M.-S.; Gariboldi, N.; Grob, S.; Skarby, P.; Paul, T.A.; Mahdizabed, N. Dielectric Insulation Medium. U.S. Patent 8,822,870 B2, 2 September 2014.
22. Kieffel, Y.; Girodet, A.; Piccoz, D.; Maladen, R. Use of a Mixture Comprising a Hydrofluoroolefin as a Medium-voltage Arc-extinguishing and/or Insulating Gas and Medium-Voltage Electrical Device Comprising Same. U.S. Patent 9,491,877, 8 November 2016.
23. Preve, C.; Piccoz, D.; Maladen, R. Validation methods of SF₆ alternatives gas. In Proceedings of the 23rd International Conference on Electricity Distribution, Lyon, France, 15–18 June 2015.
24. Pang, X.; Wu, H.; Pan, J.; Qi, Y.; Li, X.; Zhang, J.; Xie, Q. Analysis of correlation between Internal discharge in GIS and SF₆ decomposition products. In Proceedings of the IEEE International Conference on High Voltage Engineering and Application, Athens, Greece, 10–13 September 2018.
25. Katagiri, H.; Kasuya, H.; Mizoguchi, H.; Yanabu, S. Investigation of the performance of CF₃I Gas as a Possible Substitute for SF₆. *IEEE Trans. Dielectr. Electr. Insul.* **2008**, *15*, 1424–1429. [[CrossRef](#)]
26. Skaggs, S.R.; Rubenstein, R. Setting the occupational exposure limit for CF₃I. In Proceedings of the Halon Options Technical Working Conference, Albuquerque, NM, USA, 27–29 April 1999.
27. Widger, P.; Haddad, A. Analysis of gaseous by-products of CF₃I and CF₃I-CO₂ after high voltage arcing using a GCMS. *Molecules* **2019**, *24*, 1599. [[CrossRef](#)]
28. Wang, Y.; Gao, Z.; Wang, B.; Zhou, W.; Yu, P.; Luo, Y. Synthesis and dielectric properties of trifluoromethanesulfonyl fluoride: An alternative gas to SF₆. *Ind. Eng. Chem. Res.* **2019**, *58*, 21913–21920. [[CrossRef](#)]
29. Hu, S.; Wang, Y.; Zhou, W.; Qiu, R.; Luo, Y.; Wang, B. Dielectric Properties of CF₃SO₂F/N₂ and CF₃SO₂F/CO₂ Mixtures as a Substitute to SF₆. *Ind. Eng. Chem. Res.* **2020**, *59*, 15796–15804. [[CrossRef](#)]
30. Long, Y.; Guo, L.; Wang, Y.; Chen, C.; Chen, Y.; Li, F.; Zhou, W. Electron Swarms Parameters in CF₃SO₂F as an Alternative Gas to SF₆. *Ind. Eng. Chem. Res.* **2020**, *59*, 11355–11358. [[CrossRef](#)]
31. Wang, X.; Zhong, L.; Yan, J.; Yang, A.; Han, G.; Wu, Y.; Rong, M. Investigation of dielectric properties of cold C₃F₈ mixtures and hot C₃F₈ gas as Substitutes for SF₆. *Eur. Phys. J. D* **2015**, *69*, 240. [[CrossRef](#)]
32. Deng, Y.; Li, B.; Xiao, D. Analysis of the insulation characteristics of C₃F₈ gas mixtures with N₂ and CO₂ using boltzmann equation method. *IEEE Trans. Dielectr. Electr. Insul.* **2015**, *22*, 3253–3259. [[CrossRef](#)]
33. Trudinger, C.M.; Fraser, P.J.; Etheridge, D.M.; Sturges, W.T.; Vollmer, M.K.; Rigby, M.; Martinerie, P.; Mühle, J.; Worton, D.R.; Krummel, P.B.; et al. Atmospheric abundance and global emissions of perfluorocarbons CF₄, C₂F₆ and C₃F₈ since 1800 inferred from ice core, firn, air archive and in situ measurements. *Atmos. Chem. Phys.* **2016**, *16*, 11733–11754. [[CrossRef](#)]
34. Li, Y.; Zhang, X.; Xiao, S.; Chen, Q.; Tang, J.; Chen, D.; Wang, D. Decomposition Properties of C₄F₇N/N₂ Gas Mixture: An Environmentally Friendly Gas to Replace SF₆. *Ind. Eng. Chem. Res.* **2018**, *57*, 5173–5182. [[CrossRef](#)]
35. Chachereau, A.; Hösl, A.; Franck, C.M. Electrical insulation properties of the perfluoronitrile C₄F₇N. *J. Phys. D. Appl. Phys.* **2018**, *51*, 495201. [[CrossRef](#)]
36. Andersen, M.P.S.; Kytte, M.; Andersen, S.T.; Nielsen, C.J.; Nielsen, O.J. Atmospheric Chemistry of (CF₃)₂CF-C≡N: A Replacement Compound for the Most Potent Industrial Greenhouse Gas, SF₆. *Environ. Sci. Technol.* **2016**, *51*, 1321–1329. [[CrossRef](#)]
37. Zhao, M.; Han, D.; Zhou, Z.; Zhang, G. Experimental and theoretical analysis on decomposition and by-product formation process of (CF₃)₂CFCN mixture. *AIP Adv.* **2019**, *9*, 105204. [[CrossRef](#)]
38. Koch, M.; Franck, C.M. High voltage insulation properties of HFO1234ze. *IEEE Trans. Dielectr. Electr. Insul.* **2015**, *22*, 3260–3268. [[CrossRef](#)]
39. Liang, Y.; Wang, F.; Sun, Q.; Zhai, Y. Molecular structural and electrical properties of trans-1,3,3,3-tetrafluoropropene and 2,3,3,3-tetrafluoropropene under external electric fields. *Comput. Theor. Chem.* **2017**, *1120*, 79–83. [[CrossRef](#)]
40. Wang, J.; Li, Q.; Liu, H.; Huang, X.; Wang, J. Theoretical and experimental investigation on decomposition mechanism of eco-friendly insulation gas HFO1234zeE. *J. Mol. Graph. Model.* **2020**, *100*, 107671. [[CrossRef](#)] [[PubMed](#)]

41. Mantilla, J.D.; Gariboldi, N.; Grob, S.; Claessens, M. Investigation of the insulation performance of a new gas mixture with extremely low GWP. In Proceedings of the IEEE Electrical Insulation Conference, Philadelphia, PA, USA, 8–11 June 2014.
42. Simka, P.; Ranjan, N. Dielectric strength of C5 perfluoroketone. In Proceedings of the 19th International Symposium on High Voltage Engineering, Pilsen, Czech Republic, 23–28 August 2015.
43. Li, Y.; Zhang, X.; Xiao, S.; Chen, Q.; Wang, D. Decomposition characteristics of C₅F₁₀O/air mixture as substitutes for SF₆ to reduce global warming. *J. Fluor. Chem.* **2018**, *208*, 65–72. [[CrossRef](#)]
44. Preve, C.; Piccoz, D.; France, P.S.; Maladen, R. Comparison of Alternatives to SF₆ Regarding EHS and End of Life. In Proceedings of the 25th International Conference on Electricity Distribution, Madrid, Spain, 3–6 June 2019.
45. Zhuo, R.; Chen, Q.; Wang, D.; Fu, M.; Tang, J.; Hu, J.; Jiang, Y. Compatibility between C₆F₁₂O–N₂ Gas Mixture and Metal Used in Medium-Voltage Switchgears. *Energies* **2019**, *12*, 4639. [[CrossRef](#)]
46. Blázquez, S.; Antiñolo, M.; Nielsen, O.J.; Albaladejo, J.; Jiménez, E. Reaction kinetics of (CF₃)₂CFCN with OH radicals as a function of temperature (278–358 K): A good replacement for greenhouse SF₆? *Chem. Phys. Lett.* **2017**, *687*, 297–302. [[CrossRef](#)]
47. Kramer, A.; Over, D.; Stoller, P.; Paul, T.A. Fiber-coupled LED gas sensor and its application to online monitoring of ecoefficient dielectric insulation gases in high-voltage circuit breakers. *Appl. Opt.* **2017**, *56*, 4505. [[CrossRef](#)]
48. Saxegaard, M.; Seeger, M.; Kristoffersen, M.; Germany, A.; Stoller, P.; Landsverk, H. Dielectric properties of gases suitable for secondary medium voltage switchgear. In Proceedings of the 23rd International Conference on Electricity Distribution, Lyon, France, 15–18 June 2015.
49. Kuffel, E.; Zaengl, W.S.; Kuffel, J. *High Voltage Engineering Fundamentals*, 2nd ed.; Elsevier: Amsterdam, The Netherlands, 2000.
50. Maikala, R.V. Modified Beer's Law—Historical perspectives and relevance in near-infrared monitoring of optical properties of human tissue. *Int. J. Ind. Ergon.* **2010**, *40*, 125–134. [[CrossRef](#)]
51. Seader, J.D.; Henley, E.J.; Roper, D.K. *Separation Process Principles*; Wiley: Hoboken, NJ, USA, 2011.
52. Taylor, R.; Krishna, R. *Multicomponent Mass Transfer*; Wiley: Hoboken, NJ, USA, 1993.
53. Bird, R.B.; Stewart, W.E.; Lightfoot, E.N. *Transport Phenomena*, 2nd ed.; Wiley: Hoboken, NJ, USA, 2002.
54. Johnson, R.A. *Miller and Freud's Probability and Statistics for Engineers*, 9th ed.; Pearson: London, UK, 2018.
55. Fuller, E.N.; Schettler, P.D.; Giddings, J.C. A new method for prediction of binary gas-phase diffusion coefficients. *Ind. Eng. Chem.* **1966**, *58*, 18–27. [[CrossRef](#)]
56. Fuller, E.N.; Ensley, K.; Giddings, J.C. Diffusion of halogenated hydrocarbons in helium. The effect of structure on collision cross sections. *J. Phys. Chem.* **1969**, *73*, 3679–3685. [[CrossRef](#)]
57. Hu, X.; Yu, X.; Hou, H.; Wang, B. Stereo-dependent dimerization, boiling points, diffusion coefficients, and dielectric constants of E/Z-HFO-1234ze. *Int. J. Quantum Chem.* **2022**, *122*, e26848. [[CrossRef](#)]